

**Spontaneous decay of small copper-cluster anions  $\text{Cu}_n^-$  ( $n = 3-6$ ), on long time scales**K. Hansen,<sup>1,2,3,\*</sup> M. H. Stockett,<sup>2,4</sup> M. Kaminska,<sup>4,5</sup> R. F. Nascimento,<sup>4,6</sup> E. K. Anderson,<sup>4</sup> M. Gatchell,<sup>4</sup>  
K. C. Chartkunchand,<sup>4</sup> G. Eklund,<sup>4</sup> H. Zettergren,<sup>4</sup> H. T. Schmidt,<sup>4</sup> and H. Cederquist<sup>4</sup><sup>1</sup>Tianjin International Center of Nanoparticles and Nanosystems, Tianjin University, 92 Weijin Road, Nankai District, Tianjin 300072, People's Republic of China<sup>2</sup>Department of Physics and Astronomy, Aarhus University, 8000 Aarhus, Denmark<sup>3</sup>Department of Physics, University of Gothenburg, 41296 Gothenburg, Sweden<sup>4</sup>Department of Physics, Stockholm University, 10691 Stockholm, Sweden<sup>5</sup>Institute of Physics, Jan Kochanowski University, 25-369 Kielce, Poland<sup>6</sup>Centro Federal de Educacao Tecnologica Celso Suckow da Fonseca, Petropolis 25620-003, RJ, Brazil

(Received 7 January 2017; published 27 February 2017)

We have measured the spontaneous neutral particle emission from copper-cluster anions ( $\text{Cu}_n^-$ ,  $n = 3-6$ ) stored at cryogenic temperatures in one of the electrostatic ion storage rings of the Double ElectroStatic Ion Ring ExpERiment facility at Stockholm University. The measured rate of emission from the stored  $\text{Cu}_3^-$  ions follows a single power-law decay for about 1 ms but then decreases much more rapidly with time. The latter behavior may be due to a decrease in the density of available final states in  $\text{Cu}_3$  as the excitation energies of the decaying ions approach the electron detachment threshold. The emissions from  $\text{Cu}_4^-$ ,  $\text{Cu}_5^-$ , and  $\text{Cu}_6^-$  are well described by sums of two power laws that are quenched by radiative cooling of the stored ions with characteristic times between a few and hundreds of milliseconds. We relate these two-component behaviors to populations of stored ions with higher and lower angular momenta. In a separate experiment, we studied the laser-induced decay of  $\text{Cu}_6^-$  ions that were excited by 1.13- or 1.45-eV photons after 46 ms of storage.

DOI: [10.1103/PhysRevA.95.022511](https://doi.org/10.1103/PhysRevA.95.022511)**I. INTRODUCTION**

The advent of a new generation of cryogenic electrostatic ion storage devices has greatly widened the feasible time range for studies of ion decay, opening the possibility to measure decay channels that are active on very long time scales [1–7]. At the Double ElectroStatic Ion Ring ExpERiment (DESIREE) facility at Stockholm University [4,7], the 13-K operating temperature yields a residual gas pressure of roughly  $10^{-14}$  mbar, allowing for the observation of processes with characteristic decay times on the order of thousands of seconds. This development puts special emphasis on radiative cooling processes, which are expected to be the dominant decay channels for molecules and clusters at long times. Fast radiative cooling of molecular ions stored in electrostatic rings was first observed in experiments on  $\text{C}_{60}^-$  at the room-temperature ring ELISA in Aarhus [8]. These fullerene ions were then found to cool with a rate exceeding those expected for vibrational cooling by two orders of magnitude and with characteristic cooling times of several milliseconds [8]. Similarly, fast radiative cooling has been observed for anthracene cations ( $\text{C}_{14}\text{H}_{10}^+$ ) [9] stored in MINRing, a compact ion storage ring in Lyon [10]. Even faster radiative cooling rates, with corresponding time scales in the sub-millisecond range, have been measured for small carbon-cluster anions ( $\text{C}_n^-$ ,  $n = 4, 6$ ) at the Tokyo Metropolitan University (TMU) E-Ring [11]. Also at TMU, slower cooling of  $\text{C}_6\text{H}^-$  ions [11] and of  $\text{C}_5^-$  and  $\text{C}_7^-$  clusters [12–14] on millisecond time scales was again observed.

These previous experiments have revealed several unexpected features of the radiative cooling process. Of particular note is that it can proceed very effectively via electronic transitions, even for clusters as small as  $\text{C}_4^-$  [8,9,14]. It is

the availability of low-lying electronic excitations in  $\text{C}_4^-$  and  $\text{C}_6^-$  and the lack of such excitations in  $\text{C}_5^-$ ,  $\text{C}_7^-$ , and  $\text{C}_6\text{H}^-$  that makes the cooling much more efficient in the former than in the latter cases. Recently, direct evidence for the emission of photons due to transitions from the lowest electronically excited optically active state in  $\text{C}_6^-$  to the electronic ground state was reported [15]. Cooling of metal clusters is of special interest because, in addition to evaporative cooling through emission of electrons, atoms, or molecules, metal clusters can radiate and thus cool via any of the following radiative mechanisms: decay from a single particle-hole electronic excitation; excitation of a short-lived surface plasmon resonance; or by vibrational and rotational cooling. The first two are unique to clusters of metals and other systems with delocalized electrons, including carbon and carbon-based molecules. Studies of metal clusters are thus the key to understanding the importance of these types of radiative cooling processes.

Only a few radiative cooling experiments have so far been carried out using *cryogenic* electrostatic ion storage devices. These are experiments on  $\text{Al}_n^-$ ,  $n = 4-5$  clusters [16] and on  $\text{SF}_6^-$  [17] at the Cryogenic Trap for Fast ion beams (CTF), in Heidelberg, and a recent study of  $\text{Cu}_n^-$ ,  $n = 4-7$ , also in the CTF [18]. In the present paper we report measurements of the spontaneous emission rate of neutral particles from the small copper-cluster anions  $\text{Cu}_n^-$ ,  $n = 3-6$ , stored in one of the DESIREE ion-storage rings at Stockholm University [4,7]. These measurements carry information on the rates of radiative cooling processes on different time scales.

**II. EXPERIMENT**

The cluster anions were produced in a cesium-sputter ion source using a solid copper cathode and accelerated to 10 keV. A bending magnet was used to select the desired

\*klavshansen@tju.edu.cn

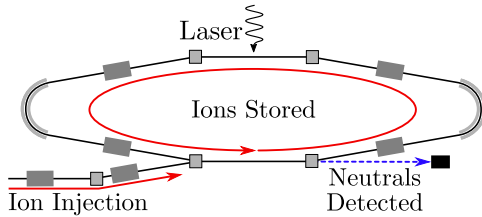


FIG. 1. One of the DESIREE storage rings with indicated charged and neutral particle trajectories. The ions were injected into the ring using a set of deflector plates. Before the ion bunch has made one turn, the voltage on the deflector was switched to a voltage such that the ion beam was stored in the ring. Neutrals from spontaneously decaying, excited  $\text{Cu}_n^-$  clusters with  $n = 3-6$  or laser-excited  $\text{Cu}_6^-$  clusters were detected by a multichannel plate detector at the end of one of the straight sections of the ring. The crossed laser beam, used for experiments with  $\text{Cu}_6^-$ , is indicated.

mass before injection into the ring. For the smallest cluster sizes, the smallest mass isotopologs were used. No sign of hydrogenation was found and for the larger clusters the most intense peak in the isotope distribution was used. Ions were injected, stored, and dumped every 0.1–10 s depending on the time scale of interest. The intrinsic ion storage lifetime in DESIREE is much longer than this, as demonstrated by measurements of metastable excited states in atomic anions where a storage lifetime of 30 min was measured for a 10-keV kinetic-energy  $\text{Te}^-$  beam [19]. For the  $\text{Cu}_n^-$ ,  $n = 3-6$  cluster anions studied here, the signal due to spontaneous decays of excited ions always becomes negligibly small within a few seconds after injection and time windows of the order of 10 s are thus sufficient in these particular cases.

In the experiment, we detected the neutral particles that were produced through electron detachment and/or unimolecular dissociation in spontaneous decay processes or, in separate experiments, from decays induced by absorption of a photon from a laser pulse. In both types of experiments, neutral particle counts were recorded as functions of time,  $t$ , with the detector placed along the line of sight of one of the straight sections of the ion-beam storage ring as shown in Fig. 1. Since the detector only registers neutral particles, it is not possible to assign the decay channel from the signal. Identification of specific decay channels is, however, not necessary for the determination of cooling times. The decay curve for  $\text{Cu}_3^-$  was recorded using time windows of 200 ms and 10 s. After normalization, the decay curves agree with each other in the region where they overlap. The spectra for  $\text{Cu}_{4,5,6}^-$  were recorded with time windows of a few seconds.

In addition to these measurements, crossed-beam laser excitation experiments were performed on  $\text{Cu}_6^-$  with the wavelengths 850 nm (1.45 eV) and 1100 nm (1.13 eV), as shown in Fig. 1. The delayed photoinduced signals for the smaller clusters were found to be significantly weaker than the ones for  $\text{Cu}_6^-$  and are not reported here. For both wavelengths the laser was fired 46 ms after injection of the  $\text{Cu}_6^-$  beam. At this time the spontaneous decay from hot clusters produced in the source has almost disappeared and the measurement is close to background free.

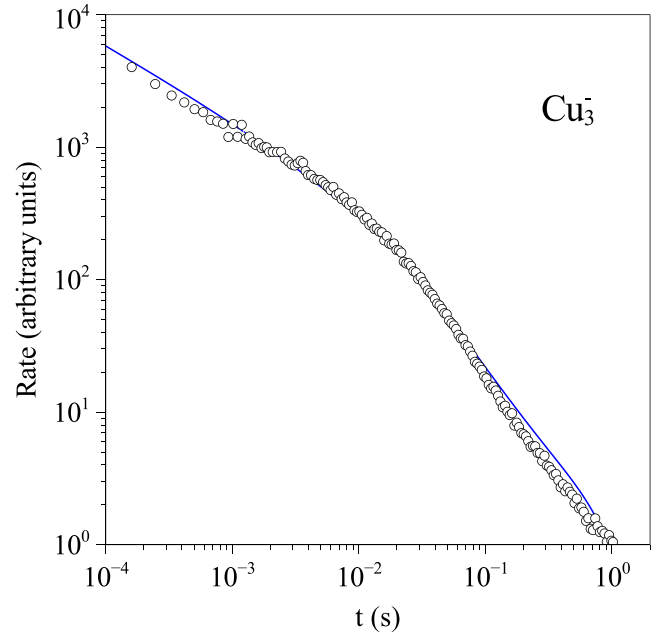


FIG. 2. Rates of neutral particles leaving a stored beam of  $\text{Cu}_3^-$  ions as functions of the time,  $t$ , after their production in the ion source. The points are measured values and the blue line is the calculated decay rate  $R(t)$  multiplied by  $t^{0.67}$  as discussed in the main text.

### III. RESULTS

#### A. Overview

Decay curves of the stored ions are shown in Figs. 2–5, in double logarithmic plots of the measured neutral emission rate for the stored ions versus the time  $t$  after production in the source. The data (recorded number of events) are binned in time intervals that increase linearly in width with  $t$ . These binned data are then divided by the width of the time bin to obtain the rate. This gives an even distribution of rate values along the horizontal axes in Figs. 2–5. The background is due to detector dark counts and collisions with residual gas. The largest component of this background is due to the detector dark counts, which has been measured separately, and which is subtracted prior to the binning of the data.

#### B. $\text{Cu}_3^-$

The  $\text{Cu}_3^-$  spectrum shown in Fig. 2 is well described by a power law at short times. At longer times the curve has a much steeper slope. This apparent two-component power-law decay could in principle be accounted for by the small number of vibrational degrees of freedom, as indicated by a direct numerical calculation. The general expression for the radiation-free spontaneous particle emission rate,  $R(t)$ , is

$$R(t) \propto \int_0^\infty g(E)k(E)e^{-k(E)t} dE, \quad (1)$$

in which  $k(E)$  is here taken to be the electron emission rate constant for ions with internal excitation energy  $E$ , and  $g(E)$  is the distribution of excitation energies. When this distribution is sufficiently broad, i.e., varies much slower with  $E$  than  $k(E)$ ,

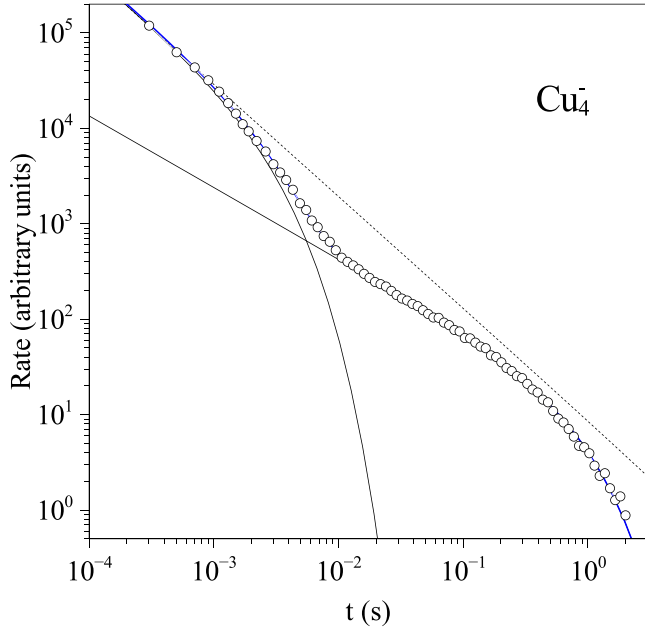


FIG. 3. Rates of neutral particles leaving a stored beam of  $\text{Cu}_4^-$ . Two quenched power-law decays are needed to fit the data. The blue line is the fit with Eq. (5), and the thin black lines are the individual contributions from the two terms in the same equation. The shortest times are excluded from the analysis for both components because the detector is saturated during the first few turns in the ring. The dotted line is the simulated decay rate without radiative cooling for a single population, calculated analogously to the line in the  $\text{Cu}_3^-$  frame. The parameters for the fits are given in Table I.

Eq. (1) can be approximated by a power-law decay rate [20]:

$$R(t) \propto t^p, \quad (2)$$

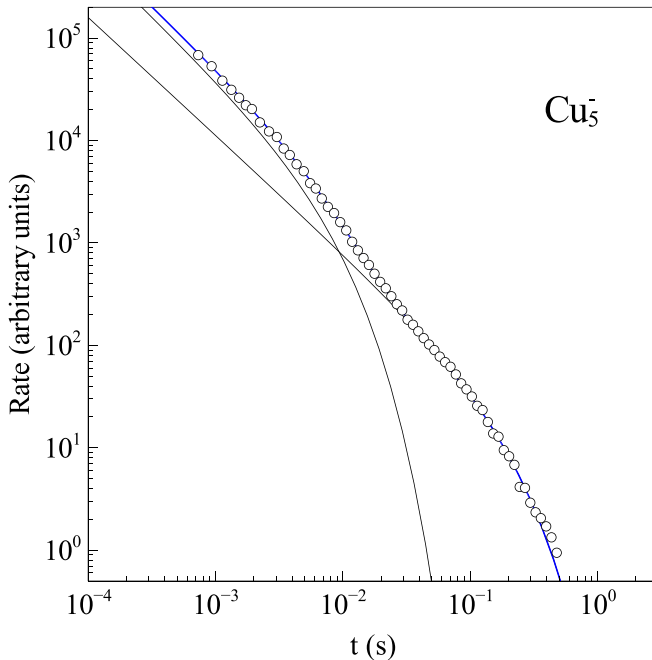


FIG. 4. Rates of neutral particles leaving a stored beam of  $\text{Cu}_5^-$  ions. The lines are analogous to the ones for Fig. 3. The parameters for the fits are given in Table I.

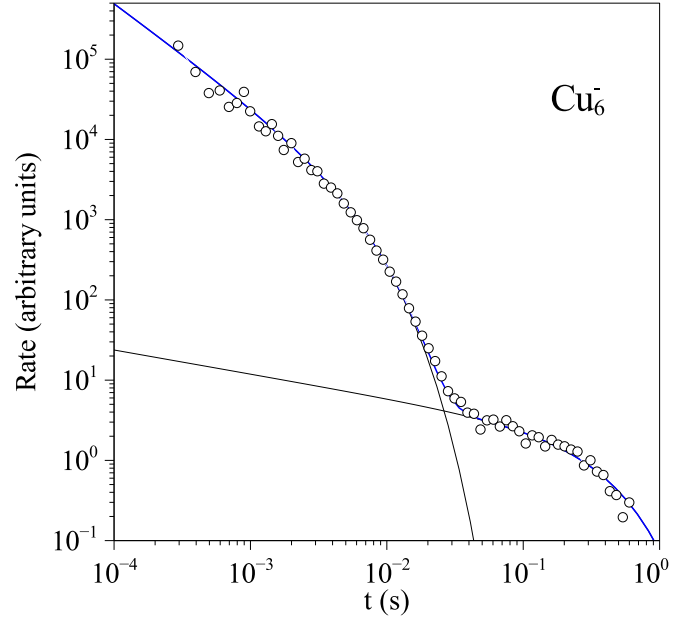


FIG. 5. Rates of neutral particles leaving a stored beam of  $\text{Cu}_6^-$  ions. The lines are analogous to the ones for Fig. 3. The parameters for the fits are given in Table I.

with  $p \approx -1$ . In general, this approximate result holds irrespective of whether the process is the statistical emission of an electron, an atom, or a molecular fragment. It may fail, however, for clusters with small heat capacities, such as  $\text{Cu}_3^-$  (see the discussion in Sec. IV C below). A quantitative estimate of the deviation from the power law in Eq. (2) requires the calculation of an explicit expression for the rate constant,  $k(E)$ , that enters into Eq. (1). Here, the calculation was done with the detailed balance rate constant for electron emission [21,22]:

$$k(E, \varepsilon) d\varepsilon = \frac{2m_e}{\pi^2 \hbar^3} \varepsilon \sigma_c \frac{\rho^{(0)}(E - E_a - \varepsilon)}{\rho^{(-)}(E)} d\varepsilon, \quad (3)$$

in which  $m_e$  is the electron mass,  $\rho^{(0)}$  and  $\rho^{(-)}$  are the level densities of the neutral and the anion,  $E$  is the  $\text{Cu}_3^-$  excitation energy,  $E_a$  is the electron affinity of  $\text{Cu}_3$ ,  $\sigma_c$  is the  $\text{Cu}_3$  electron capture cross section, and  $\varepsilon$  is the kinetic energy of the decay channel—effectively the kinetic energy of the electron. The factor of 2 in Eq. (3) accounts for the spin degeneracy of the emitted electron. The level densities were calculated with the Beyer-Swinehart algorithm [23] using the following four vibrational frequencies determined by density functional theory [Becke three-parameter Lee-Yang-Parr and Los Alamos National Laboratory two-double-z (B3LYP/LANL2DZ)]: 230, 142, and 52  $\text{cm}^{-1}$  (doubly degenerate). The same frequencies were used for both  $\text{Cu}_3$  and  $\text{Cu}_3^-$ . For the electron affinity, which acted as the activation energy, the experimental value 2.45 eV [24] was used. The electron attachment cross section,  $\sigma_c$ , was set to the constant value of  $1.5 \times 10^{-21} \text{ m}^2$ . This small cross section is strongly reduced from the Langevin value as an assumed effect of a small electron-cluster sticking coefficient. This assumption is made here as the density of states in  $\text{Cu}_3^-$  may well be very low due to a very narrow range of electron energies. In the calculation of the total rate constant,  $\varepsilon$  is integrated out by a numerical summation over

the states,

$$k(E) = \sum_i k(E, \varepsilon_i) \delta \varepsilon, \quad (4)$$

in which the sum runs over the discretized values of  $\varepsilon$  and  $\delta \varepsilon$  is the energy resolution of the level density defined by the Beyer-Swinehart calculation. In addition to the rate calculated by numerical integration of Eq. (1) with the rate constant from Eqs. (3) and (4), the calculated function,  $R(t)$ , is multiplied by the time to the power 0.67 in Fig. 2. This power is a fit factor which could possibly be related to the shape of the excitation energy and angular momentum distributions of the clusters produced in the source.

We assign the deviation from a single power-law decay behavior of  $\text{Cu}_3^-$  to the low density of vibrational states in neutral  $\text{Cu}_3$  close to the vibrational ground state. The crossover from one slope to the other could be a result of the freezing out of a single vibrational degree of freedom. However, both slopes will be too steep without the fit factor  $t^{0.67}$ . Furthermore, the second part of the curve requires the electrons to be captured in the inverse process with the reduced Langevin cross section mentioned above. The effect of the reduction is to postpone the freezing out of the last vibrational degree of freedom and instead make the next-to-last freezing out observable in the experimental time window. Apart from this last shift, the mechanism proposed is similar to the one made in connection with the CTF study of  $\text{SF}_6^-$  in Heidelberg [17]. The main difference to those data is that not all final-state vibrations freeze-out at the same excitation energy in the copper trimer. Therefore the decay may continue to follow a power law but with a different slope than at earlier times.

Finally, we note a very slight change in the slope for the experimental data at times longer than 0.1 s in Fig. 2. A weak component from a second distribution of internal energies of  $\text{Cu}_3^-$  that could be due to trimer ions with different conformations and/or angular momentum distributions cannot be ruled out.

### C. $\text{Cu}_{4,5,6}^-$

The measured neutral particle emission signals for  $\text{Cu}_4^-$ ,  $\text{Cu}_5^-$ , and  $\text{Cu}_6^-$  are more complex than that of  $\text{Cu}_3^-$ . For  $\text{Cu}_4^-$  the measurements span more than four orders of magnitude in time (see Fig. 3), and for  $\text{Cu}_5^-$  and  $\text{Cu}_6^-$  the range is nearly four orders of magnitude in time (see Figs. 4 and 5).

A calculation similar to the one for  $\text{Cu}_3^-$  shows a qualitatively similar effect for  $\text{Cu}_4^-$ , albeit so strongly reduced that the decay rate is very close to a single power law (see the dotted line in Fig. 3), and therefore it cannot explain the experimental data. For  $\text{Cu}_4^-$ ,  $\text{Cu}_5^-$ , and  $\text{Cu}_6^-$ , the data are instead well represented by a sum of two curves:

$$R(t) = a_1 t^{-1+\delta_1} e^{-t/\tau_1} + a_2 t^{-1+\delta_2} e^{-t/\tau_2}. \quad (5)$$

As mentioned above, the power-law decay at short times is an effect of the broad internal energy distribution of the cluster ions from the source [20], and the exponential decay is the consequence of radiative cooling.

## IV. DISCUSSION

### A. Role of angular momentum

The existence of two components of the decay curves for  $\text{Cu}_{4,5,6}^-$  will be discussed in terms of two distinct populations of ions, characterized by different angular momenta. The observation of two beam components with very different lifetimes will then be linked to a conserved quantity that effectively preserves the integrity of the two populations, and endows them with distinct and conserved properties. Of primary importance for the following reasoning are the different lowest-energy geometries of species with different angular momenta. The sputter source that we use is of a type known to produce dimer and larger anions in high rotational states [16,17,25–27], and this is most likely the case also in the present experiment. We therefore tentatively assign the two characteristic times for each of the three cluster sizes  $n = 4, 5, 6$  to species with higher and lower angular momentum.

The suggested mechanisms are discussed with the aid of Fig. 6. In this figure we show relative excitation energies for  $\text{Cu}_3^-$  and  $\text{Cu}_4^-$  ions in different conformations and as functions of their rotational angular momenta,  $J$ , with cluster structures from density-functional theory calculations (B3LYP/LANL2DZ). These energies are given relative to the energies of the most stable nonrotating isomers of  $\text{Cu}_3^-$  and  $\text{Cu}_4^-$  in their vibrational ground states. For each anion conformation there are progressions of vibrational states from the yrast line and upward. Conformers can convert into each other as long as energy and angular momentum are conserved, but the higher-energy conformer populations are suppressed by their small level densities relative to those of the ground states.

Copper trimer anions in states with total excitation energies and  $J$  values above the lowest gray line in the upper panel of Fig. 6 may decay through electron detachment or through fragmentation. The latter process is, however, most likely slowed down as it leaves the product with only a single vibrational degree of freedom while electron emission gives products with four vibrational degrees of freedom. Electron detachment will thus be entropically favored in this upper region of energies and  $J$  values. Trimer anions with total energies below the same gray line, but above the dot-dashed lines, may only decay through dissociation channels.

For the  $\text{Cu}_4^-$  ions, the situation is more complicated. There are three conformer detachment limits that are close in energy and mostly lie above the fragmentation limits as indicated in the lower panel in Fig. 6. The three conformers have linear, rhombic, and Y-shaped forms with the detachment limit for the linear one being highest in energy for all values of  $J$  below 500. The detachment limits for the rhombic and Y-shaped forms cross near  $J = 400$ ; the latter has the lowest energy for  $J > 400$  while the rhombic form is lower in energy for  $J < 400$ . There is a region of total and rotational energies where  $J < 300$  and where the detachment limit for the rhombic form lies below the lowest fragmentation limit. Only electron detachment processes are possible in this ( $J < 300$ ) region.

These relations between conformer detachment limits for  $\text{Cu}_3^-$  and  $\text{Cu}_4^-$  indicate that the decay behaviors can be different for  $\text{Cu}_4^-$  ions in low and high rotational states while

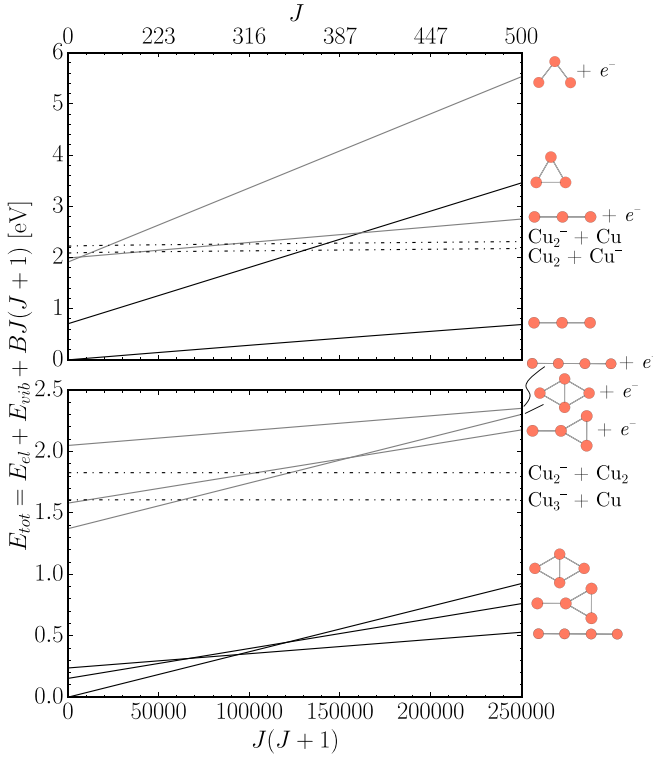


FIG. 6. Calculated relative excitation energies (black lines) for two  $\text{Cu}_3^-$  (upper panel) and three  $\text{Cu}_4^-$  (lower panel) conformers in their lowest vibrational states as functions of  $J(J+1)$  where  $J$  is the rotational angular momentum quantum number. The corresponding electron detachment limits (full gray lines) and the lowest-energy fragmentation channels (dash-dotted lines) are also indicated. There are progressions of vibrational states (not indicated) from the lowest state (black lines) of each conformation, reaching into the continuum beyond the corresponding detachment limit. No states exist below the lowest black line in each plot (the yrast line). Ions in excited states that are below both the lowest-energy detachment limit and the lowest dissociation limit are bound and cannot produce neutrals. The rotational barrier heights for the fragmentation channels increase with  $J$  and the dash-dotted lines should in principle have small nonzero slopes. We have calculated this effect for the dissociating  $\text{Cu}_3^-$  clusters, but the effect is not visible on the scale shown here (the same is expected to be true for  $\text{Cu}_4^-$ ).

such a situation is less likely to occur for  $\text{Cu}_3^-$ . In this scenario, it is possible that the two distributions that appear in the data for  $\text{Cu}_4^-$  (see Fig. 3) are related to detachment from Y-shaped anions above  $J = 400$  and detachment from rhombic anions for  $J < 400$ , respectively. However, when we also consider the fragmentation channels—assuming for the moment that the corresponding rates are not negligible in relation to the present experimental time scales—we note that fragmentation is the lowest-energy channel leading to neutral products for  $J > 300$  while the detachment limit is lowest in energy for  $J < 300$  in  $\text{Cu}_4^-$ . The situation is different for  $\text{Cu}_3^-$  where fragmentation has the lowest excitation energy (or close to) over a much wider range of  $J$  values. In any case, it appears that different parts of the distribution, belonging to ions in high and low  $J$  states, may give rise to the double structures that we measure in the decay of  $\text{Cu}_4^-$ .

Summarizing the suggested explanation, we have seen that the trimer decay can be explained without invoking two populations, consistent with the linear ground-state structure seen in quantum chemical calculations including the present ones. The larger clusters with theoretically more compact ground states, on the other hand, display double decay curves, consistent with anionic clusters belonging to two populations with different angular momenta and conformations—linear (or Y-shaped) species at high  $J$  and more compact (rhombic) species at low  $J$ . At the high angular momenta the neutral  $\text{Cu}_4^-$  clusters may be rhombic or Y shaped, depending on the precise value of  $J$ . These trends for  $\text{Cu}_4^-$  are likely to apply to the two larger clusters, also, as these are not expected to be linear for low  $J$  values.

## B. Radiative cooling

We now turn to the quasiexponential decrease of the  $\text{Cu}_4^-$ ,  $\text{Cu}_5^-$ , and  $\text{Cu}_6^-$  decay curves after a few milliseconds, ascribed to radiative cooling. Radiative cooling, i.e., photon emission from excited vibrational [28], electronic [9], or plasmonic [8] states, depletes the population of hot ions without producing neutral particles and effectively quenches the power-law decay rate. Depending on the magnitude of the energies of the emitted photons, the resulting spontaneous decay rate may vary either as [20]

$$R(t) \propto \frac{t^\delta}{e^{t/\tau} - 1}, \quad (6)$$

which is valid for small photon energies, or as [14]

$$R(t) \propto t^{-1+\delta} e^{-t/\tau}, \quad (7)$$

for larger photon energies. Here, “large” photon energies are those for which the emission of a single photon suppresses any further unimolecular decay. For short times,  $t \ll \tau$ , both expressions reduce to the power law,  $R \propto t^p$ , with  $p = -1 + \delta$ , and for long times to a quasiexponential decay.

The photon energy required to quench the decay can be compared with the vibrational energy quantum. The (room-temperature) Debye temperature of bulk copper is 310 K [29], corresponding to a quantum energy of 0.027 eV. Even for emission of such a comparatively low-energy photon, the effect for the present clusters will be a quenching of further unimolecular decay, corresponding to a decay rate following Eq. (7) [13]. For electronic transitions, the quenching effect is even stronger because of the much larger energies of the emitted photons. In either case, we can use Eq. (7) for the fits of the data reported here. The fitted effective quenching times,  $\tau$ , then directly give the photon emission rate constants without any further analysis.

The fitted radiative time constants in Table I are mean values of the thermally populated, vibrationally excited states. The detailed balance expression for the photon emission rate constant,  $k_p$ , can be represented as [22,30]

$$k_p(E) = \int \frac{8\pi\nu^2}{c^2} \sigma_{abs}(\nu) \frac{\frac{\rho(E-h\nu)}{\rho(E)}}{1 - \frac{\rho(E-2h\nu)}{\rho(E-h\nu)}} d\nu, \quad (8)$$

in which  $\nu$  is the cyclic frequency of the emitted photon and  $c$  is the speed of light. We have assumed an excitation energy independent absorption cross section,  $\sigma_{abs}(\nu)$ . Finally,  $\rho$  is the

TABLE I. Parameters for  $\text{Cu}_n^-$  decay curves fitted to Eq. (5). The power-law exponent  $p$  is equal to  $-1 + \delta$ . The magnitudes of the time constants indicate that they are due to vibrational transitions. Uncertainties from the fits are  $\pm 0.05$  for the  $\delta$ 's and between 10 and 20% for the lifetimes. Vertical detachment energies, VDEs, from Ref. [24] are given in the right column.

$N$	Short		Long		VDE (eV)
	$\delta$	$\tau$ (ms)	$\delta$	$\tau$ (ms)	
4	-0.1	2.6	0.25	830	1.45
5	-0.2	7.5	-0.15	180	1.94
6	-0.28	5.9	0.7	330	1.96

level density, calculated with all modes except the emitting states. From the expression it is clear that thermal photon emission is an activated process. The broad energy distribution and resulting spread in the radiative rate constant may therefore potentially render the radiative decay nonexponential, in analogy to the nonradiative electron emission. The effect will, however, not appear here because the radiative rate constant,  $k_p$ , is much less energy dependent than the unimolecular decay constant, and a description in terms of an energy independent photon emission rate constant is a very good approximation. For an illustration of this point, see Fig. 3 of [14].

The shorter of the characteristic cooling times for  $\text{Cu}_4^-$  (2.6 ms), for  $\text{Cu}_5^-$  (7.5 ms), and for  $\text{Cu}_6^-$  (5.9 ms) are all rather close to each other. These lifetimes, as well as their associated power-law exponents  $p = -1 + \delta$  discussed below, are very similar to those measured for  $\text{Al}_4^-$  and  $\text{Al}_5^-$  [16]. These ions were also produced with a sputter source and stored in a cryogenic ion-beam trap. Time constants of several milliseconds are expected for vibrational transitions, which suggests emission of infrared photons as the source of this cooling. The assignment of the two different time constants requires a more detailed analysis which is outside the scope of this paper.

### C. Power-law exponents

Turning finally to the question of the initial power-law decay, we address the deviations of  $p$  from minus unity. The fitted values for the spontaneous decay of the three largest clusters are summarized in Table I. We see that the size dependence of the rate constants does not seem to be influenced in any significant way by the well-known shell structure and odd-even effects observed in abundances of copper-cluster anions [31], and also does not seem to reflect the vertical detachment energies [24] (last column in Table I). The power is expected to be less than  $-1$  for small clusters. In the simplest case, when  $g(E)$  in Eq. (1) is constant and the heat capacity is not too small, the exponent  $p$  is close to  $-1$ . Including the effect of the finite heat capacity gives [20,22,28]

$$p \equiv -1 + \delta \approx -1 - \frac{1}{C} - \frac{2}{C} \times \frac{e^{-\ln(\omega t)/C}}{1 - e^{-\ln(\omega t)/C}} \quad (9)$$

in which  $C$  is the effective microcanonical heat capacity in units of  $k_B$  and  $\omega$  is the frequency factor in the rate constant of this channel.

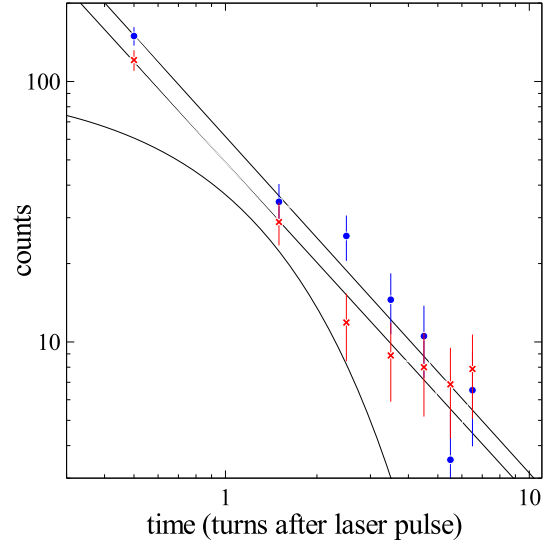


FIG. 7. A double-logarithmic plot of the photoinduced decay of  $\text{Cu}_6^-$  at the two wavelengths 850 nm (blue circles) and 1100 nm (red crosses). The time unit is the revolution period for the  $\text{Cu}_6^-$  ions in the ring which is  $\sim 120 \mu\text{s}$ . The straight lines are power-law fits. For comparison, an exponential decay with the lifetime of one period is plotted (curved line).

Although the short-time  $\delta$ 's are negative as expected, the quantitative agreement with Eq. (9) is poor. This is even more pronounced for the slow component, where the value is large and positive for  $\text{Cu}_6^-$ . This suggests that the values may be influenced by the excitation energy distributions produced in the source. The idea can be further investigated by comparing the value of  $\delta$  measured in photoexcitation experiments as the absorption of a photon and the resulting enhanced decay probes the cluster's energy distribution at an excitation energy which is smaller than the energy at which the spontaneous decay occurs.

The rates of decay of the signal induced by absorption of photons at the wavelengths 850 and 1100 nm in  $\text{Cu}_6^-$  are shown in Fig. 7. These two measurements show power-law decays with exponents that are very similar:  $-1.29 \pm 0.08$  for the 850-nm measurement and  $-1.28 \pm 0.07$  for the 1100-nm measurement yielding a weighted average of  $-1.28 \pm 0.05$ . This is identical to the value of  $\delta$  in Table I from the spontaneous decay at short times. If the energy of the clusters that decay spontaneously is denoted by  $E_0$ , the distributions are thus probed at the three energies  $E_0$ ,  $E_0 - 1.13$  eV, and  $E_0 - 1.45$  eV, yielding similar  $\delta$  values. Given that  $E_0$  is close to the threshold, these three points span a significant part of the distribution. We thus conclude that a value of  $\delta$  of  $-0.28$  reflects a property of the clusters themselves and not a property of the production process, i.e., not of the distribution  $g(E)$ .

It should be noted that laser excitation experiments, also on  $\text{Cu}_6^-$ , with photon energies of 1.165 eV (1064 nm) gave a time-dependent exponent starting at  $\sim -1.2$  at short times and reaching  $-0.8$  at 2 s [18]. The change is ascribed to radiative cooling and the related change of the excitation energy distribution. The energy distribution was found to agree with a canonical distribution with an initial temperature of 1100 K

(for times between 0.02 and 0.3 s). The canonical energy distribution at this temperature changes slowly with energy at the energies probed in the experiments. Consequently, the  $\delta$  value measured for these times and photon energies should be essentially free from corrections from the energy distribution and reflect intrinsic cluster properties. This is consistent with the conclusions made above.

The present value,  $\delta = -0.28$ , for  $\text{Cu}_6^-$  is, however, and as already mentioned, not consistent with Eq. (9). The equation gives  $-0.09$ , and a direct simulation for  $\text{Cu}_6^-$ , analogous to that for  $\text{Cu}_3^-$ , gives values between  $-0.10$  and  $-0.11$  for electron detachment and atomic evaporation, respectively. We conclude that the measured value of  $\delta$  is influenced by (as yet undetermined) factors intrinsic to the cluster, beyond the properties of the model used here. It is not clear to what degree this conclusion holds for the other cluster sizes.

## V. SUMMARY

In summary, we have measured the spontaneous decay of small copper-cluster anions  $\text{Cu}_n^-$  with  $n = 3-6$ . We observe a complex decay behavior with two power-law decays each with their characteristic radiative lifetimes for  $\text{Cu}_4^-$ ,  $\text{Cu}_5^-$ , and  $\text{Cu}_6^-$ . We do not observe radiative cooling for  $\text{Cu}_3^-$ . We tentatively identify the two populations for  $n = 4-6$  with cluster anions with lower and higher rotational excitations. For the higher rotational energies, elongated conformers have the lowest total energies for  $n = 4, 5, 6$ , while lower rotational energies tend to give more compact structures. The borders between the regions appear to lie at angular momenta of a few hundred units of  $\hbar$ , corresponding to rotational energies of a few tenths of an eV. The trimer anion does not exhibit the two-component decay seen for the tetra-, penta- and hexamer. This is reasonable because the linear form of the anion has the lowest total energy for all values of the angular momentum quantum number. Remarkably, no electronic cooling was observed in any of

the measured clusters, which would have been manifested as sub-milli-second cooling times. The deviation of the initial power-law decay for  $n = 4-6$  from  $-1$  is only partly explained by the small heat capacity and seems to have contributions from unknown factors intrinsic to the clusters as indicated by the probing of distinctly different parts of the initial excitation energy distribution for  $\text{Cu}_6^-$  by means of laser excitation.

As to the origin of the two angular momentum distributions for  $n = 4-6$ , that we tentatively have identified with the two-component decay behaviors, we note the following. The radiative cooling time for each component depends on the geometry of the stored cluster anions. Provided the channel that dominates the signal at short times also has the shortest radiative decay time, this is sufficient to produce a two-component decay. Minority components with short decay times will remain unobserved. The values of the  $\delta$ 's depend also on the precise decay channel, in the first instance through the number of vibrational degrees of freedom in the product. Different geometries may have different values for that number, and the curves may therefore also depend on the crossing of energy curves in the upper part of the frames in Fig. 6.

## ACKNOWLEDGMENTS

This work was supported by the Swedish Research Council (Contracts No. 821-2013-1642, No. 621-2015-04990, No. 621-2014-4501, No. 621-2013-4084, and No. 2016-06625) and by the Knut and Alice Wallenberg Foundation. We acknowledge support from the COST Action No. CM1204 XUV/X-ray light and fast ions for ultrafast chemistry (XLIC). M.K. acknowledges financial support from the Mobility Plus Program (Project No. 1302/MOB/IV/2015/0) funded by the Polish Ministry of Science and Higher Education. K.H. acknowledges grants from the University of Gothenburg Faculty of Science Strategic Initiative, and from Aarhus Universitets Forskningsfond.

- 
- [1] P. Reinhed, A. Orbán, J. Werner, S. Rosén, R. D. Thomas, I. Kashperka, H. A. B. Johansson, D. Misra, L. Brännholm, M. Björkhage, H. Cederquist, and H. T. Schmidt, *Phys. Rev. Lett.* **103**, 213002 (2009).
- [2] P. Reinhed, A. Orbán, S. Rosén, R. D. Thomas, I. Kashperka, H. A. B. Johansson, D. Misra, A. Fardi, L. Brännholm, M. Björkhage, H. H. Cederquist, and H. T. Schmidt, *Nucl. Instrum. Methods A* **621**, 83 (2010).
- [3] M. Lange, M. Froese, S. Menk, J. Varju, R. Bastert, K. Blaum, J. R. Crespo Lopez-Urrutia, F. Fellenberger, M. Grieser, R. von Hahn, O. Heber, K. U. Kühnel, F. Laux, D. Orlov, M. L. Rappaport, R. Repnow, C. D. Schröter, D. Schwalm, A. Shornikov, T. Sieber, Y. Toket, J. Ullrich, A. Wolf, and D. Zajfman, *Rev. Sci. Instrum.* **81**, 055105 (2010).
- [4] R. D. Thomas, H. T. Schmidt, G. Andler, M. Björkhage, M. Blom, L. Brännholm, E. Bäckström, H. Danared, S. Das, N. Haag, P. Halldén, F. Hellberg, A. I. S. Holm, H. A. B. Johansson, A. Källberg, G. Källersjö, M. Larsson, S. Leontein, L. Liljeby, P. Löfgren, B. Malm, S. Mannervik, M. Masuda, D. Misra, A. Orbán, A. Paál, P. Reinhed, K. G. Rensfelt, S. Rosén, K. Schmidt, F. Seitz, A. Simonsson, J. Weimer, H. Zettergren, and H. Cederquist, *Rev. Sci. Instrum.* **82**, 065112 (2011).
- [5] R. von Hahn, F. Berg, K. Blaum, J. R. Crespo Lopez-Urrutia, F. Fellenberger, M. Froese, M. Grieser, C. Krantz, K. U. Kühnel, M. Lange, S. Menk, F. Laux, D. Orlov, R. Repnow, C. D. Schröter, S. Shornikov, T. Sieber, J. Ullrich, A. Wolf, M. Rappaport, and D. Zajfman, *Nucl. Instrum. Methods B* **269**, 2871 (2011).
- [6] Y. Nakano, W. Morimoto, T. Majima, J. Matsumoto, H. Tanuma, H. Shiromaru, and T. Azuma, *J. Phys.: Conf. Ser.* **388**, 142027 (2012).
- [7] H. T. Schmidt, R. D. Thomas, M. Gatchell, S. Rosén, P. Reinhed, P. Löfgren, L. Brännholm, M. Blom, M. Björkhage, E. Bäckström, J. D. Alexander, S. Leontein, D. Hanstorp, H. Zettergren, L. Liljeby, A. Källberg, A. Simonsson, F. Hellberg, S. Mannervik, M. Larsson, W. D. Geppert, K. G. Rensfelt, H. Danared, A. Paál, M. Masuda, P. Halldén, G. Andler, M. H. Stockett, T. Chen, G. Källersjö, J. Weimer, K. Hansen, H. Hartman, and H. Cederquist, *Rev. Sci. Instrum.* **84**, 055115 (2013).

- [8] J. U. Andersen, C. Brink, P. Hvelplund, M. O. Larsson, B. Bech Nielsen, and H. Shen, *Phys. Rev. Lett.* **77**, 3991 (1996).
- [9] S. Martin, J. Bernard, R. Brédy, B. Concina, C. Joblin, M. Ji, C. Ortega, and L. Chen, *Phys. Rev. Lett.* **110**, 063003 (2013).
- [10] J. Bernard, G. Montagne, R. Brédy, B. Terpend-Ordacière, A. Bourgey, M. Kerleroux, L. Chen, H. T. Schmidt, H. Cederquist, and S. Martin, *Rev. Sci. Instrum.* **79**, 075109 (2008).
- [11] G. Ito, T. Furukawa, H. Tanuma, J. Matsumoto, H. Shiromaru, T. Majima, M. Goto, T. Azuma, and K. Hansen, *Phys. Rev. Lett.* **112**, 183001 (2014).
- [12] M. Goto, A. E. K. Sundén, H. Shiromaru, J. Matsumoto, H. Tanuma, T. Azuma, and K. Hansen, *J. Chem. Phys.* **139**, 054306 (2013).
- [13] K. Najafian, M. S. Pettersson, B. Dynefors, H. Shiromaru, J. Matsumoto, H. Tanuma, T. Furukawa, T. Azuma, and K. Hansen, *J. Chem. Phys.* **140**, 104311 (2014).
- [14] N. Kono, T. Furukawa, H. Tanuma, J. Matsumoto, H. Shiromaru, T. Azuma, K. Najafian, M. S. Pettersson, B. Dynefors, and K. Hansen, *Phys. Chem. Chem. Phys.* **17**, 24732 (2015).
- [15] Y. Ebara, T. Furukawa, J. Matsumoto, H. Tanuma, T. Azuma, H. Shiromaru, and K. Hansen, *Phys. Rev. Lett.* **117**, 133004 (2016).
- [16] M. W. Froese, K. Blaum, F. Fellenberger, M. Grieser, M. Lange, F. Laux, S. Menk, D. A. Orlov, R. Repnow, T. Sieber, Y. Toker, R. von Hahn, and A. Wolf, *Phys. Rev. A* **83**, 023202 (2011).
- [17] S. Menk, S. Das, K. Blaum, M. W. Froese, M. Lange, M. Mukherjee, R. Repnow, D. Schwalm, R. von Hahn, and A. Wolf, *Phys. Rev. A* **89**, 022502 (2014).
- [18] C. Breitenfeldt, K. Blaum, M. W. Froese, S. George, G. Guzmán-Ramírez, M. Lange, S. Menk, L. Schweikhard, and A. Wolf, *Phys. Rev. A* **94**, 033407 (2016).
- [19] E. Bäckström, D. Hanstorp, O. M. Hole, M. Kaminska, R. F. Nascimento, M. Blom, M. Björkhage, A. Källberg, P. Löfgren, P. Reinhed, S. Rosén, A. Simonsson, R. D. Thomas, S. Mannervik, H. T. Schmidt, and H. Cederquist, *Phys. Rev. Lett.* **114**, 143003 (2015).
- [20] K. Hansen, J. U. Andersen, P. Hvelplund, S. P. Møller, U. V. Pedersen, and V. V. Petrunin, *Phys. Rev. Lett.* **87**, 123401 (2001).
- [21] V. Weisskopf, *Phys. Rev.* **52**, 295 (1937).
- [22] K. Hansen, *Statistical Physics of Nanoparticles in the Gas Phase*, Springer Series on Atomic, Optical, and Plasma Physics Vol. 73 (Springer, Dordrecht, 2013).
- [23] T. Beyer and D. F. Swinehart, *Commun. ACM* **16**, 379 (1973).
- [24] D. G. Leopold, J. Ho, and W. C. Lineberger, *J. Chem. Phys.* **86**, 1715 (1987).
- [25] J. Fedor, K. Hansen, J. U. Andersen, and P. Hvelplund, *Phys. Rev. Lett.* **94**, 113201 (2005).
- [26] O. Aviv, Y. Toker, D. Strasser, M. L. Rappaport, O. Heber, D. Schwalm, and D. Zajfman, *Phys. Rev. A* **83**, 023201 (2011).
- [27] B. Kaffle, O. Aviv, V. Chandrasekaran, O. Heber, M. L. Rappaport, H. Rubinstein, D. Schwalm, D. Strasser, and D. Zajfman, *Phys. Rev. A* **92**, 052503 (2015).
- [28] J. U. Andersen, H. Cederquist, J. S. Forster, B. A. Huber, P. Hvelplund, J. Jensen, B. Liu, B. Manil, L. Maunoury, S. Brøndsted Nielsen, U. V. Pedersen, H. T. Schmidt, S. Tomita, and H. Zettergren, *Eur. Phys. J. D* **25**, 139 (2003).
- [29] C. Ho, R. Powell, and P. Liley, *J. Phys. Chem. Ref. Data* **3**, 1 (1974).
- [30] J. U. Andersen, E. Bonderup, and K. Hansen, *J. Phys. B: At. Mol. Opt. Phys.* **35**, R1 (2002).
- [31] I. Katakuse, T. Ichihara, Y. Fujita, T. Matsuo, T. Sakurai, and H. Matsuda, *Int. J. Mass Spectrom. Ion Processes* **74**, 33 (1986).